Spanish Journal of Agricultural Research
18 (3), e1204, 13 pages (2020)
eISSN: 2171-9292
https://doi.org/10.5424/sjar/2020183-16269
Instituto Nacional de Investigación y Tecnología Agraria y Alimentaria (INIA)

RESEARCH ARTICLE

OPEN ACCESS

Improving the monitoring of corn phenology in large agricultural areas using remote sensing data series

Ernesto Sifuentes-Ibarra (Sifuentes-Ibarra, E)[1], Waldo Ojeda-Bustamante (Ojeda-Bustamante, W)[2], Ronald E. Ontiveros-Capurata (Ontiveros-Capurata, RE)[3] and Ignacio Sánchez-Cohen (Sánchez-Cohen, I)[4]

[1] INIFAP, Campo Experimental Valle del Fuerte. Carretera internacional México-Nogales km 1609, Juan José Ríos, Sinaloa 81110, Mexico. [2] Colegio Mexicano de Ingenieros en Irrigación, Vicente Garrido No. 106, Cuernavaca, Morelos 62000, México. [3] CONACYT-Instituto Mexicano de Tecnología del Agua (IMTA), Subcoordinación de Ingeniería de Riego. Paseo Cuauhnáhuac 8532, Progreso, Jiutepec, Morelos 62550, México. [4] INIFAP, Centro Nacional de Investigación Disciplinaria en Relación Agua-Suelo-Planta-Atmósfera. Km. 6.5 Margen derecha canal de Sacramento, Gómez Palacio, Durango 35150, Mexico.

Abstract

Aim of study: Mexico's large irrigation areas demand non-structural actions to improve the irrigation service, such as monitoring crop phenology; however, its application has been limited by the large volumes of field information generated, diversity of crop management and climatic variability. The objective of this study was to generate and validate a methodology to monitor corn (*Zea mays* L.) phenology from the historical relationship of the vegetation indexes (VIs), EVI and NDVI, with the phenological development (PD) of corn grown in large irrigation zones.

Area of study: Irrigation District (ID) 075 "Valle del Fuerte", northern Sinaloa, Mexico.

Material and methods: We used a database of 20 years of climate, field crop growth and crop phenology data, and Landsat satellite images. A methodology was proposed on a large scale supported with GIS and remote sensing data series.

Main results: The methodology was validated in 19 plots with an acceptable correlation between observed PD and estimated PD for the two VIs, with slightly better values for EVI than for NDVI. NDVI and EVI models agreed with experimental PD observations in 92.1% of the farms used to validate the methodology, in 2.5% only the NDVI model coincided with the real, in 3.1% only the EVI model coincided, and in 2.3% both models disagreed with observation, generated a stage out of phase with respect to the real phenological stage.

Research highlights: is possible to generalize the methodology applied to large irrigation zones with remote sensing data and GIS.

Additional key words: *Zea mays* L.; irrigation districts; climate variability; GIS; Mexico

Abbreviations used: AW (Autum-Winter season); C (Cold); CGDD (Cumulative Growing Degree Days); EVI (Enhanced Vegetation Index); GDD (Growing Degree Days); GIS (Geographic Information Systems); H (Hot); ID (Irrigation District); IM (Irrigation Module); N (Neutral); NDVI (Normalized Difference Vegetation Index); PD (Phenological Development); Ta (air daily mean temperature); Tm (mean temperature); VARI (Visible Atmospherically Resistant Index); VI (Vegetation Index); WUA (Water Users Association)

Authors' contributions: ESI: paper writing and fieldwork for validation plots, as well as calculations and processing of satellite images. WOB: defined the paper structure, applied methodology, and the application of the CGDD concept to monitor phenology in large irrigation areas using remote sensing. REOC: reviewed the phenological application of spectral vegetation indexes and radiometrically and atmospherically images correction. ISC: document reviewed and defined the phenological field monitoring.

Citation: Sifuentes-Ibarra, E; Ojeda-Bustamante, W; Ontiveros-Capurata, RE; Sánchez-Cohen, I (2020). Improving the monitoring of corn phenology in large agricultural areas using remote sensing data series. Spanish Journal of Agricultural Research, Volume 18, Issue 3, e1204. https://doi.org/10.5424/sjar/2020183-16269

Received: 19 Dec 2019. **Accepted:** 05 Aug 2020.

Funding agencies/institutions	Project / Grant
Mexican Sectorial Funding SADER-CONACYT	Plataforma Informativa sobre Usos del Agua en la Agricultura Nacional

Competing interests: The authors have declared that no competing interests exist.

Correspondence should be addressed to Waldo Ojeda-Bustamante: w.ojeda@riego.mx

Introduction

In Mexico, more than six million hectares are annually irrigated, representing almost a third of the agricultural area cultivated, and generating 50% of the total value of agricultural production (SIAP, 2019). Mexican irrigation zones (IZs) institutionally are classified in 86 Irrigation Districts (IDs) integrated by Irrigation Modules (IMs)

and managed by Water Users Associations (WUAs), and 50735 Irrigation Units (IUs) that users operate autonomously (CONAGUA, 2019a,b).

One of the main problems of these large areas is the low irrigation efficiencies (30 to 45%) at farm level, associated with poor irrigation service by WUAs and poor conduction efficiency (Sifuentes *et al.*, 2015). To improve irrigation efficiency and service, detailed knowledge of the phenological development of crops is required to better couple irrigation to crops' water demand that change with their phenological development (Espinosa *et al.*, 2017). Although efforts have been made to implement farm monitoring of crop phenology in Mexico's IDs, its application has been limited due to the large quantity of irrigated areas, diversity of crops and high volumes of field information that are managed (Ojeda-Bustamante *et al.*, 2007). In a scenario of high competition for limited resources, coupled with food security and the effects of climate change, agricultural monitoring becomes very important (Heupel *et al.*, 2018).

The Growing Degree Day (GDD) concept has been used for several decades to estimate the phenological crop stages for corn (*Zea may*s L.) (Ojeda-Bustamante *et al.*, 2006), wheat (*Triticum aestivum* L.) (Kimball *et al.*, 2012) and potato (*Solanum tuberosum* L.) (Flores *et al.*, 2012), among others; however, its application depends on the knowledge of accurate agronomic and environmental information such as sowing date, type and variety crop, air daily temperature (Ta) and a non-restrictive development management such as the absence of water, nutritional or environmental stress (Roth & Yocum, 1997; Ghamghami *et al.*, 2019; Hufkens *et al.*, 2019).

The use of remote sensing to identify and classify crops is currently a common task, using their spectral characteristics (Heupel *et al.*, 2018). However, its practical application to estimate other agricultural variables remains a major challenge due to the high heterogeneity and size of cultivated farms, the presence of clouds and spatial resolution of images (Burke & Lobell, 2017; Hufkens *et al.*, 2019). Vegetation Indices (VIs), defined as mathematical combinations or transformations of two or more bands of the electromagnetic spectrum to maximize vegetation characteristics (Tsouros *et al.*, 2019), are the most widely used products of remote sensing to estimate crop phenology (Kamble *et al.*, 2013; Zhong *et al.*, 2014). The VIs most commonly used have been reported to be the Normalized Difference Vegetation Index (NDVI) and the Enhanced Vegetation index (EVI) (Matsushita *et al.*, 2007). De Bernardis *et al.* (2016) fitted functions of phenological development data and NDVI values to predict the rice (*Oryza sativa* L.) phenology. Reed *et al.* (1994) used historical series of NDVI obtained from Advanced-Very-High-Resolution-Radiometer images to predict wheat phenology; Wei *et al.* (2019) used EVI and NDVI indices to monitor the phenology of 12 crops in large areas reporting an accuracy of 85% and 81%, respectively.

Remote sensing also allows monitoring the actual crop conditions in the field with adequate spatial and temporal resolution. When the cumulative growing degree days (CGDD) are coupled with the VIs, phenological monitoring is significantly improved (Mavi & Tupper, 2004; Teal *et al.*, 2006). Viña *et al.* (2004) reported a good fit of the Visible Atmospherically Resistant Indices (VARIs), $VARI_{green}$ and $VARI_{red\text{-}edge}$, and NDVI with the corn CGDD and chlorophyll content. The VARIs were more sensitive than the NDVI with respect to the green fraction of vegetation cover, improving the detection of senescence, vegetative development and presence of various types of stress. Liao *et al.* (2019) used the cumulative temperature in the parameters related to a phenology model and information extracted from Landsat-8 and MODIS images to simulate growth and biomass production in corn and soybeans (*Glycine max* L.).

Landsat satellite image time series is an alternative for monitoring crops in large agricultural areas, with a moderate spatial and temporal resolution (30 m and 16 days respectively). They are freely accessible with enough information for use and application (Ghamghami *et al.*, 2019; NASA, 2019). However, in Mexico studies focused on developing practical methodologies for monitoring crop phenology are scarce. Moreover, the sowing period and corn genotypes have changed drastically in the last decade in the northwest of Mexico, so this type of tool to monitor crop phenology is a recurrent demand. The objective of this study was to generate and validate a methodology to monitor corn phenological using vegetation indices, validated with historical data obtained from field and meteorological data and Landsat satellite images of 20 agricultural years; this was done in the largest Mexican ID, where corn is the dominant crop.

Material and methods

Study area

This study was carried out in an area of approximately 20,000 ha located at the union of the IMs "Santa Rosa" and "Batequis" in ID075 "Valle del Fuerte" in the northern region of the state of Sinaloa Mexico, located in the coordinates 25°45'N and -108° 51'W (Fig. 1). The ID075 is the largest in the country, with more than 260,000 ha harvested annually and a production value about 850 million U.S. dollars, with more than 170,000 ha of corn with an average yield of 12.7 t ha^{-1} and a production value of 400 million U.S. dollars (SIAP, 2019), the study area records an average annual rainfall of 352 mm, average annual temperature of 25 °C and an altitude of 15 m.a.s.l. The soils are flat, deep, with no problem of salts and mostly with clay and

Figure 1. Location of the study area

loam clay textures with available moisture in the range of 0.143 to 0.155 $cm^3\ cm^{-3}$ (UAS, 2014).

Thirty commercial corn farms that had a detailed historical record of at least twenty agricultural years (1998-2018) were selected as reference in the study area, 20 farms located in the IM Santa Rosa (240.8 ha) and 10 in the IM "Batequis" (120 ha).

Climatic seasonal analysis

This arid region shows high climatic variability, which impacts the phenology and season duration of crops. To obtain more information on this effect, an analysis of seasonal climatic variability in the corn phenological was carried out with respect to a typical growing season from November 12 to April 14 of the following year. This approach was performed to classify each agricultural season: Hot (H), Neutral (N) or Cold (C), according to the CGDD during this fixed period of 152 days, wich corresponds to the duration in CGDD from sowing to maturation in the study area with November 12 as the sowing date (INIFAP, 2017). In this way, a cold season is defined as when the CGDD value in the 152 days was from 1100 to 1200, a neutral season when the value was from 1201 to 1300 GDD and for a hot season when the value was more than 1300 CGDD.

Historical series of Landsat images

A total of 116 Landsat satellite images (5, 7 and 8) were downloaded for the analysis period (USGS, 2018) (https://glovis.usgs.gov/), which were corrected radiometrically and atmospherically to improve both, position and radiometric quality, according to the methodology proposed by Chander *et al.* (2009) for Landsat 5 and 7, and USGS (2019) for Landsat 8 (OLI/TIRS). The annual period analyzed was seven months (November to May), which corresponds to the main agricultural season Autumn-Winter (AW) of the study area, where the presence of clouds is reduced. Fig. 2 shows the type and number of Landsat images used.

Historical relationship VIs-CGDD

In order to analyze the historical behavior of VIs-CGDD, the first step was to estimate the CGDD value in each reference farm for each available satellite image. Complementary data, as sowing, harvest and irrigation data, as well as agronomic and management data, were extracted from the SPRITER system as detailed and applied by Ojeda-Bustamante *et al.* (2007) in the study zone. To estimate the CGDD, a historical series (1998-2018) of air daily mean temperature (Ta) was used from an automated meteorological station operated by the Instituto Nacional de Investigaciones Forestales, Agrícolas y Pecuarias (INIFAP) located in the center of the study area. The GDD calculation was performed using the following equation applied in the study area (Ojeda-Bustamante *et al.*, 2006):

$$\begin{aligned} GDD &= T_a - Tc_{min}, \text{ if } T_a < Tc_{max}\ ; \\ GDD &= Tc_{max} - Tc_{min}, \text{ if } T_a \geq Tc_{max}\ ; \\ GDD &= 0, \text{ if } T_a \leq TC_{min} \end{aligned} \quad (1)$$

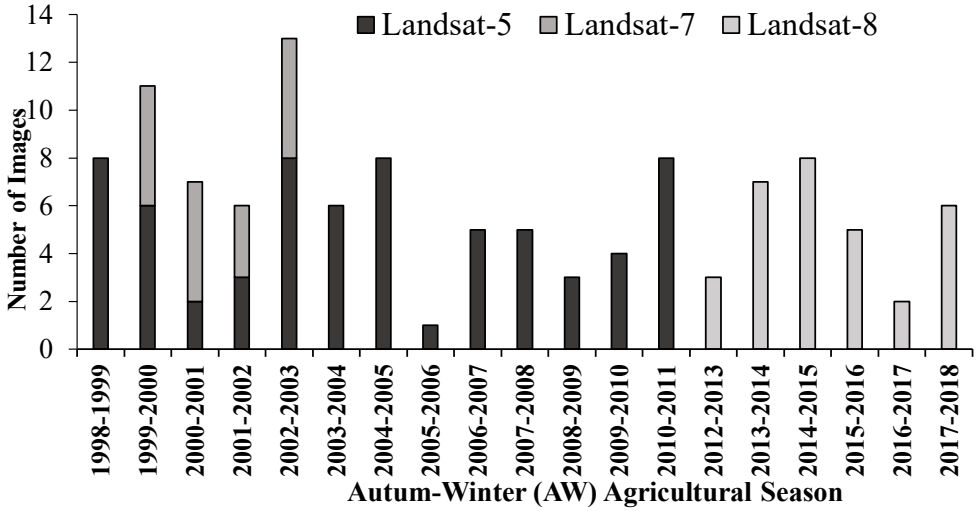

Figure 2. Number and type of Landsat images used in the study area

where GDD are the daily growing degree days (ºC day^{-1}), T_a is the average daily air temperature calculated from records of 15 minutes (ºC), Tc_{max} is the maximum critical temperature of the corn crop (30 ºC) and Tc_{min} is the minimum critical temperature of the corn crop (10 ºC). With CGDD values, the phenological development (PD) was calculated as a development ratio using equation (2):

$$PD = \frac{CGDD_{ID}}{CGDD_{Maturity}} \quad (2)$$

where $CGDD_{ID}$ are the GDD accumulated from the sowing date to the interest date (ºC) and $GDD_{Maturity}$ is the GDD accumulated from the sowing date to crop physiological maturity (1451 CGDD) (ºC).

After that, using the raster calculation and "Area Statistics Calculation" tools of the QGIS (2019), the VI averages for each reference farm on each image date were calculated to be associated with the CGDD. The expressions for the calculation of the VIs used were those indicated by Rouse *et al.* (1974) for the NDVI (3) and by Huete *et al.* (2002) for the EVI (4).

$$NDVI = \frac{\rho_{NIR} - \rho_{red}}{\rho_{nir} + \rho_{red}} \quad (3)$$

$$EVI = 2.5\left[\frac{\rho_{nir} - \rho_{red}}{\rho_{nir} + 6\rho_{red} - 7.5\rho_{blue} + 1}\right] \quad (4)$$

where ρ_{NIR} is the average reflectance in the near-infrared band (840 to 880 nm), ρred is the average reflectance in the red band (620 to 670 nm) and ρ_{blue} the average reflectance in the blue band (460 to 480 nm).

Finally, a statistical fitting analysis was done among the values of the two VIs with PD. Table 1 shows the CGDD intervals with their corresponding phenological phases and PD values for each range for most hybrids in the study area, characterization based on the methodology reported by Ritchie *et al.* (1992) and in the studies carried out by Ojeda-Bustamante *et al.* (2006).

Methodological approach

The proposed methodology is based on the estimation of PD as a function of VIs, using historical series of Landsat satellite images and phenological field data. The step sequence was the following (as shown in Fig. 3):

1. Compilation of climate data and reference farm data.
2. Download the Landsat image series for the dates of interest from a remote sensing website with historical satellite images (*i.e.* https://glovis.usgs.gov/).
3. Calibration and radiometric correction of satellite images according to the methodology described previously.
4. Calculation of VIs with Geographic Information Systems (GIS) software for each reference farm data using the corresponding multispectral-satellite image (*i.e.* QGIS).
5. Estimation of PD using reference-farm data based on CGDD with equation (2) and Table 1 using several agricultural years (Table 2).
6. Estimation of PD as a function of VIs using the fitted quadratic equations (Table 3) or using Table 4. Make sure to locate PD in the correct zone of crop development, in the ascending zone (I) if current VI (VI_i) is greater than previous VI (VI_{i-1}), in the descending zone (II) if current VI (VI_i) is less than previous VI (VI_{i-1}).

Table 1. Phases of development, cumulative growing degree days (CGDD, ºC) and phenological development (PD) (%/100) for the most used corn hybrids in the north of Sinaloa, Mexico.

Phases of development	CGDD	PD
1-2 leaves (V1-V2)	200-300	0.14-0.21
3-4 leaves (V3-V4)	300-400	0.21-0.28
4-6 leaves (V4-V6)	400-500	0.28-0.34
6-8 leaves (V6-V8)	500-600	0.34-0.41
8-11 leaves (V8-V11)	600-700	0.41-0.48
11 leaves-tasseling (V11-VT)	700-800	0.48-0.55
Tasseling-silking (VT-R1)	800-900	0.55-0.62
Blister-milk stage (R2-R3)	900-1100	0.69-0.76
Milk stage-dough stage (R3-R4)	1100-1200	0.76-0.83
Dough stage-dent stage (R4-R5)	1200-1300	0.83-0.90
Dent stage-physiological maturitv(R5-R6)	1300-1400	0.90-0.96
Physiological maturity (R6)	1400-1500	0.96-1-03
Harvest stage (H)	1600-1700	1.10-1.17

7. Map generation with the estimated phenological development (PD), using either quadratic equations (Table 3) or Table 4 for zone I and zone II.

Validation

The phenological phases determined with CGDD (from sowing to image date) were compared against the stages observed weekly in the fields. This was done for 19 of the 30 reference plots established with corn during the AW 2017-2018 season. Field information from these plots (farms) was also used to validate the spectral models. The accuracy of the large-scale methodology was determined in the total of corn farms in two different dates of the IM Batequis for the agricultural season AW 2017-2018. It was determined by comparing the observed PD with the predicted by the model.

Results and discussion

Historical behavior of crop development

Fig. 4 shows the behavior of the historical development of the corn crop in the reference farms associated with CGDD. Each point is the value of CGDD from sowing to the date of the image. The high variability in the behavior of the series is related to climatic variability among years and sowing dates, which is consistent with Ojeda-Bustamante *et al.* (2014), who estimated increase of at least 1.2 ºC in the annual mean temperature for northern Sinaloa for the first third of this century with respect to the base period (1951-2000), as a result of a possible effect of climate change. In C (Cold) years, the series' trend showed a lower slope due to a lengthening of the season, in H (Hot) years the slope is more vertical as a result of a shortening of the season, while for N (Neutral)

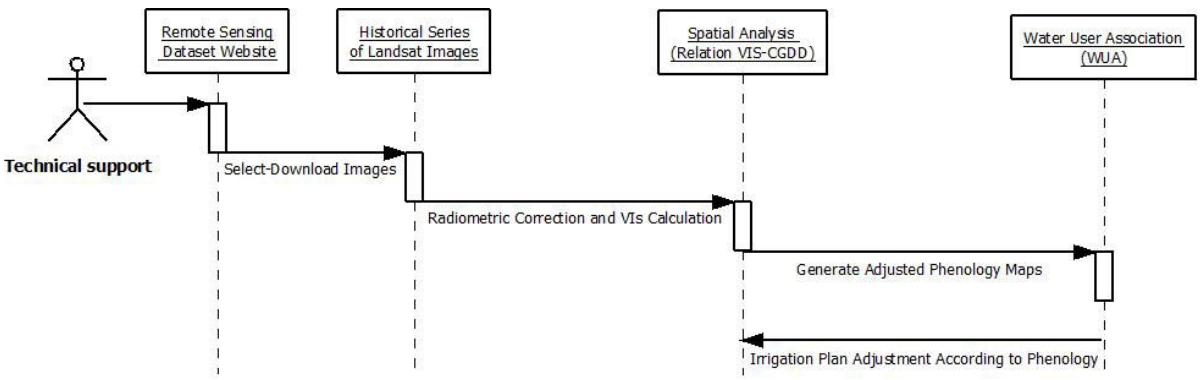

Figure 3. Sequential scheme of the generated methodology

Table 2. Years classification [Cold (C), Normal (N) and Hot (H)] to indicates the historical effect of temperature on the phenological development of corn as expressed in CGDD and season duration in days, established in three sowings periods (early, typical and late sowing) for the agricultural years analyzed

Agricultural year	Type	Early			Late			Typical		
		CGDD	Tm	Duration	CGDD	Tm	Duration	CGDD	Tm	Duration
1998-1999	C	1409	19.3	158	1245	18.2	165	1150	17.6	177
1999-2000	N	1329	18.8	165	1378	19.1	157	12230	18.1	169
2000-2001	N	1326	18.8	165	1388	19.2	156	1247	18.3	168
2001-2002	N	1411	19.3	157	1456	19.6	152	1272	18.4	165
2002-2003	H	1440	19.5	154	1520	20.0	148	1384	19.1	157
2003-2004	N	1265	18.3	170	1282	18.4	163	1182	17.8	174
2004-2005	N	1479	19.8	149	1329	18.7	160	1219	18.0	172
2005-2006	N	1353	18.9	164	1459	19.6	152	1214	18.0	172
2006-2007	C	1299	18.5	167	1226	18.1	167	1151	17.6	177
2007-2008	C	1203	17.9	175	1234	18.1	168	1143	17.5	178
2008-2009	H	1474	19.7	150	1418	19.3	154	1300	18.6	165
2009-2010	H	1374	19.0	160	1374	19.0	157	1279	18.4	167
2010-2011	C	1204	17.9	175	1271	18.4	166	1142	17.5	176
2011-2012	C	1247	18.2	174	1303	18.6	162	1137	17.5	176
2012-2013	N	1240	18.2	172	1305	18.6	162	1180	17.8	176
2013-2014	H	1381	19.1	160	1384	19.1	156	1256	18.3	167
2014-2015	H	1463	19.6	151	1427	19.4	154	1300	18.6	165
2015-2016	H	1478	19.8	150	1414	19.3	154	1354	18.9	161
2016-2017	H	1591	20.5	138	1478	19.7	150	1381	19.1	158
2017-2018	H	1629	20.7	130	1528	20.1	147	1428	19.4	154
Mean		1380	19.1	159	1371	19.0	158	1247	18.2	169

CGDD: cumulative growing degree days (º C) from sowing to 152 days after sowing. Tm: air average temperature (º C) from sowing to 152 days after sowing. Duration: crop season duration (days)

Table 3. Parameters for equation $PD=f(VI)=\alpha_1 \pm [\alpha_2+(\alpha_3*VI)]^{0.5}$ form, for $VI \leq VI_{max}$, otherwise $PD=PD_{VT}$, to estimate phenological development (PD) as a function of vegetation indices (VIs) considering two zones of corn development. Zone I: equation with negative sign (-) for the square root. Zone II: equation with positive sign (+) for the square root.

PD = f (VI)	Parameter			VI_{max}	PD_{VT}	R^2
	α_1	α_2	α_3			
PD_{NDVI}	0.6130	0.3740	-0.5150	0.726	0.607	0.7059
PD_{EVI}	0.6191	0.3106	-0.4052	0.767	0.616	0.6975

seasons, the slope is intermediate. Table 2 shows a more detailed historical analysis, where the effect of the sowing date and temperature on the duration of crop phenological season is observed.

For early (October), typical (November) and late (December) sowing periods, it was possible to quantify the CGDD historical variation and the mean temperature (Tm), calculated for a fixed interval of 152 days from sowing to physiological maturity, as well the elapsed time expressed in days after sowing to maturity (DAS). In the early and late sowing periods, high CGDD values were observed due to the effect of high temperature at the beginning and the end of crop seasons respectively, which reduced the duration of crop phenological season. On the

Table 4. Minimum and maximum values of NDVI and EVI and their relationship with phenological development (PD) and stages of corn, located in two zones and at the maximum point of the development curve, used for large-scale phenological monitoring.

Zone	NDVI		EVI		PD	Phases of development
	min	max	min	max		
I	0.26	0.31	0.19	0.26	0.14-0.21	V1-V2
	0.32	0.50	0.27	0.41	0.21-0.28	V3-V4
	0.51	0.60	0.42	0.57	0.28-0.34	V4-V6
	0.61	0.67	0.58	0.69	0.34-0.41	V6-V8
	0.68	0.73	0.70	0.81	0.41-0.48	V8-V11
Peak	**0.74**	**0.74**	**0.82**	**0.82**	**0.48-0.55**	**V11-VT**
II	0.69	0.73	0.73	0.81	0.55-0.62	VT-R1
	0.65	0.68	0.65	0.72	0.69-0.76	R2-R3
	0.63	0.64	0.61	0.64	0.76-0.83	R3-R4
	0.59	0.62	0.56	0.6	0.83-0.90	R4-R5
	0.51	0.58	0.50	0.55	0.90-0.96	R5-R6
	0.44	0.50	0.40	0.49	0.96-1-03	R6
	0.27	0.43	0.25	0.39	1.10-1.17	Harvest

other side, the typical or conventional sowing dates produced the largest crop duration due to colder temperatures. The warming trend found in the last five years compared to previous 15 agricultural years, had a reduction of up to 24 days, which represents a 13% reduction when compared to the phenological duration at the beginning of the analyzed period; this effect was also reported by Castillo & Ibáñez (2017). In consequence, there is an inverse relation between Tm and CGDD, the more Tm is related to a lesser CGDD. The high inter and intra-seasonal variability suggest an improvement crop phenology monitor to better coupling crop water demands, in large irrigation zones.

The comparison between the phenological development estimated with CGDD in the dates of the images and the observed growth in the sowings of 19 farms for the AW season 2017-2018 is shown in Fig. 5, where a high correlation can be observed between the values observed with those estimated with an RMSE of 0.029 corresponding to 2.9% (4.5 days) of the total development; the value of one corresponds to the physiological maturity of the crop and values higher than this are farms close to harvest.

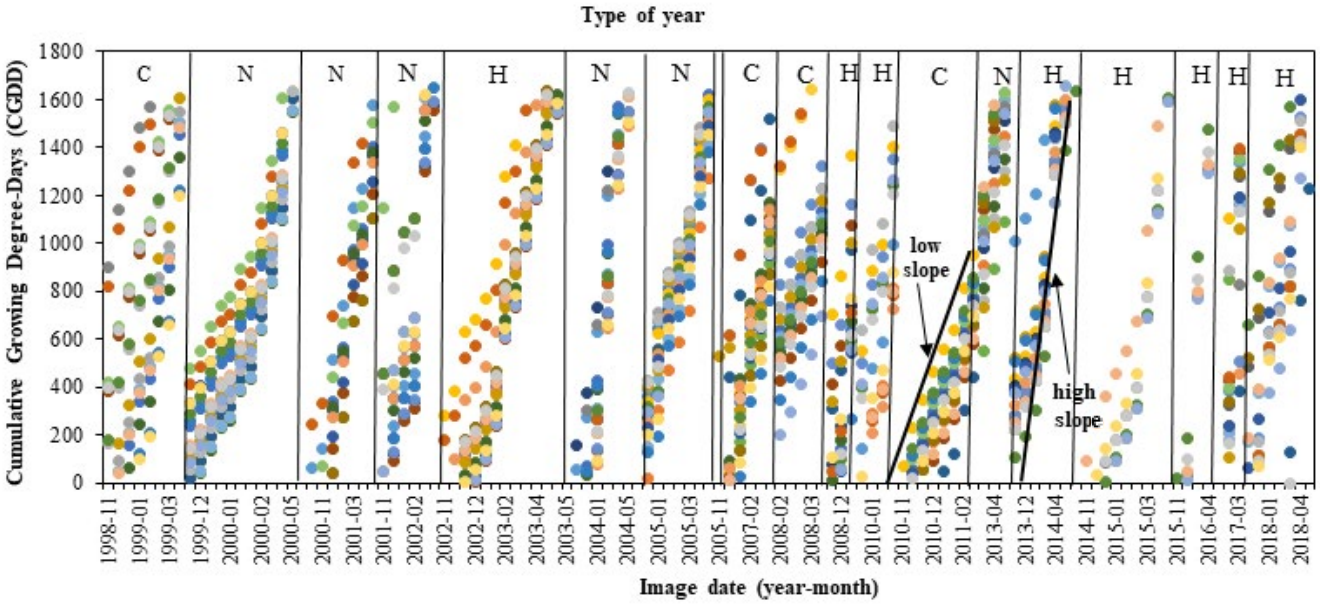

Figure 4. Cumulative growing degree-days (CGDD) in Autumn-Winter (AW) seasons for each Landsat image in reference farms, as a reference, each crop-farm is shown in a unique color and the type of year as cold (C), normal (N) and hot (H) in years analyzed.

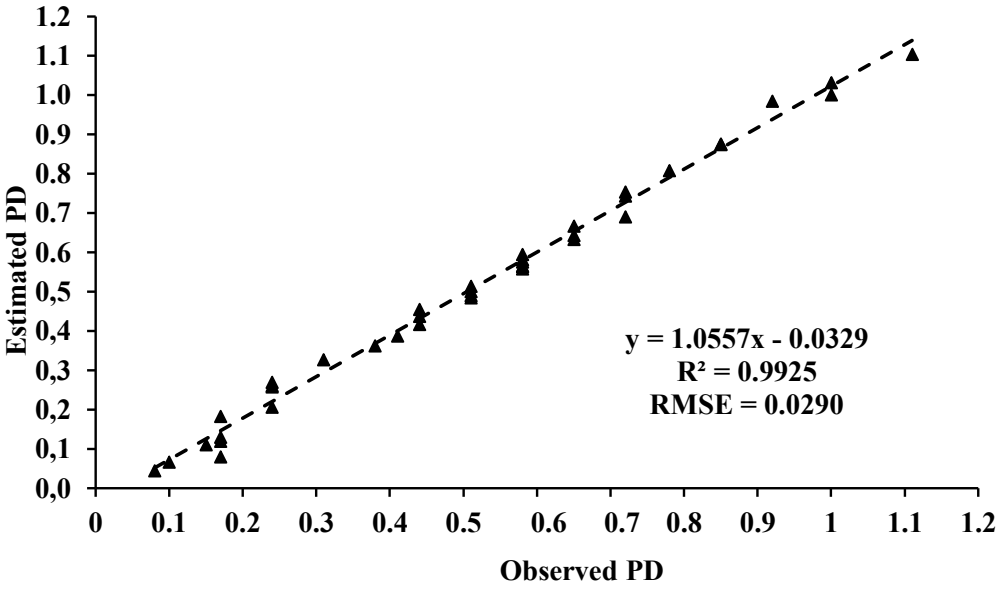

Figure 5. Comparison of estimated crop development with cumulative growing degree days (CGDD) on Landsat image and development observed on corn reference farms (Autum-Winter 2017-2018 season), Phenological Development (PD) calculated as the ratio of daily CGDD and CGDD until physiological maturity

Spectral models

Fig. 6 shows the PD as a function of the two VIs. It is observed a points dispersion due to variability in crop management and crop stress; Viña *et al.* (2004) mentioned that the use of VIs through remote sensors makes it possible to detect some symptoms of crop stress that most crop growth and development models do not recognize. A higher dispersion range can be observed in the zone of maximum development or peak zone in EVI (0.6-1.0) than in NDVI (0.6-0.8), probably due to the higher capacity of EVI for the detection of stressed fields in the same phase of crop development. It is also observed that after the maximum value (PD = 0.61), the VIs values have a decreasing behavior and are similar to the values before the maximum PD. To express PD as a unique function of VIs, the curve was divided into two zones (Fig. 6): zone I (upward, from sowing to VI peak) and zone II (falling, from VI peak to harvest). The fitted model for the calculation of PD as a function of VIs for the two zones were derived from the roots of a second-order equations (obtained from PD-VIs data), where VI corresponds to the independent variable and the PD to the dependent variable. Equation parameters for both zones are indicated in the Table 3.

Another option to calculate PD as a function of VI is by using a tabular format. Table 4 shows the interval of NDVI and EVI values for each interval of phenological stages as well as the values of PD in the interval, which were obtained from Fig. 6; the location zone is also indicated. The peak VIs, estimated with the fitted model, are also reported. The first four phases the values of NDVI are slightly higher than those of EVI, while from the fifth to the ninth phase EVI values are greater than NDVI values; while in the last four phases EVI was lower than NDVI. This behavior was also reported by Wei *et al.* (2019), indicating that it was due to the higher sensitivity of the EVI to high biomass, bare soil, and senescence than the NDVI. EVI showed higher response with high biomass for PD = 0.54 (800 CGDD) and in the senescence stage of the crop from PD = 0.69 after 1000 CGDD. This is also seen in Fig. 7 representing the relationship of the two indices studied, as suggested by Huete *et al.* (2002) and Jensen (2007). This figure also indicates the relevance of estimating either of the two indices from the value of one of these, due to its high determination coefficient.

GIS-based phenology monitoring

To implement the spectral models in a GIS an algorithm was generated, to automatically estimate PD for each cornfield of the IM, from VIs values calculated using multispectral-satellite images. To find out the zone (Fig. 6 and Table 4), an indicator was obtained when subtracting the value of a previous date image (VI_{i-1}) with the current VI_i; positive values correspond to Zone I and negative values correspond to Zone II. An algorithm was implemented in Visual Basic language to calculate the PD in the total of cornfields as a function of the VIs, subsequently these results were incorporated into the GIS to visualize them spatially.

Methodology precision

The validation results of the models in the 19-reference farms for AW 2017-2018 season was done by using the

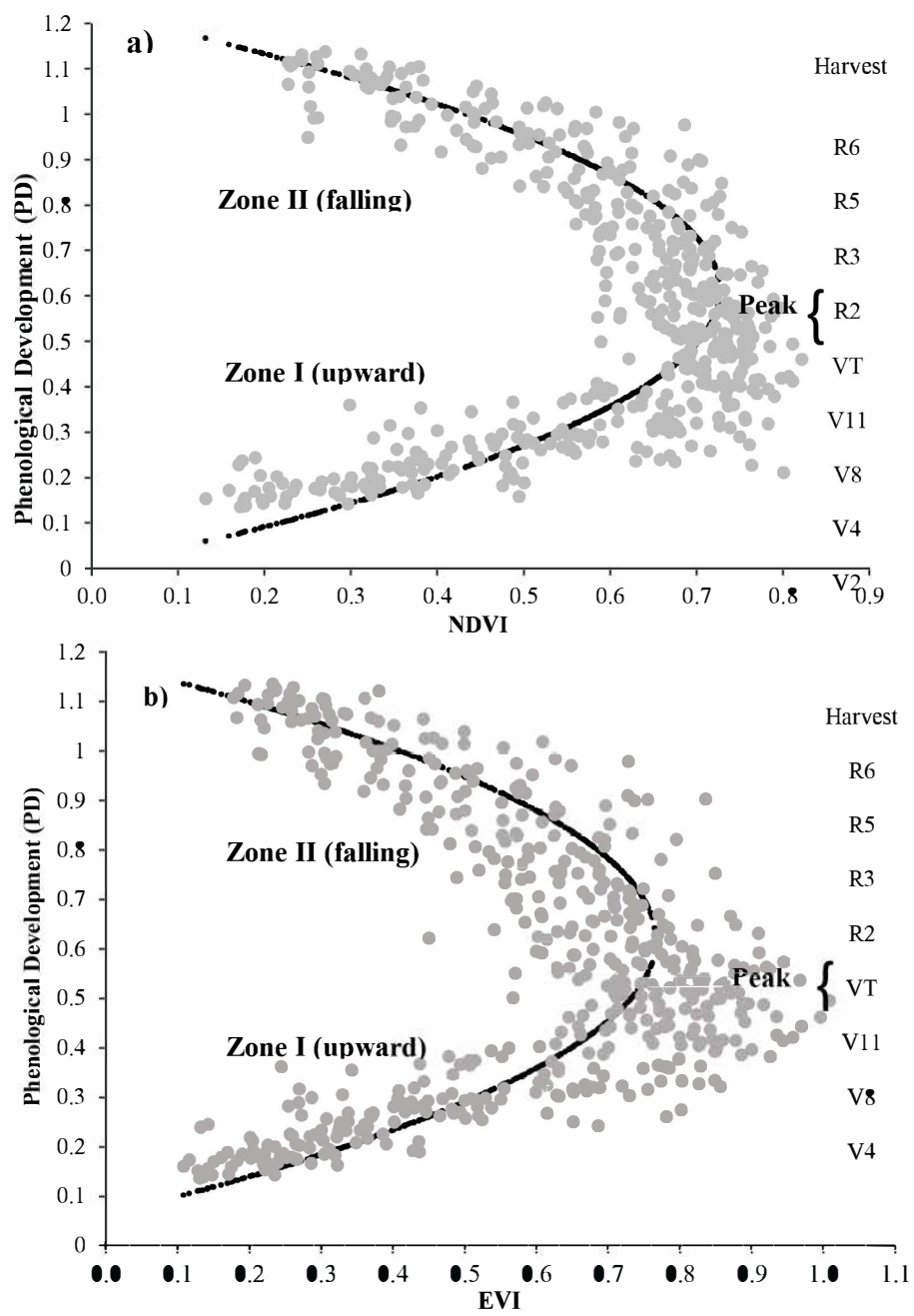

Figure 6. Historical NDVI (a) and EVI (b) values and its relationship with phenological development (PD) for corn, in the north of Sinaloa, Mexico

equation parameters indicated on Table 3 and shown in Fig. 8. A determination coefficient (R^2) of 0.9154 for the NDVI model and of 0.9124 for EVI, with RMSE values of 0.1307 and 0.1219, respectively, were estimated. The values indicated good precision for both models, however the effect of the point´s dispersion and the spatial and temporal variability in the 19 farms distributed in the 20,000 ha of the study area was also reflected, mainly when the value was greater than peak value estimated by the model. This influenced the precision to estimate phenology as reported by Burke & Lobell (2017) and Hufkens *et al.* (2019).

Fig. 9 shows the actual phenology (a) and the validation of the spectral models (b), at IM to two contrasting moments of crop development (beginning and end of the season) generated with a GIS, and using Table 4 in the algorithm. At the first moment (January 11, 2018), Fig. 9 (above), the corn farms were predominantly in phases V6-V8, V8-V11 and V11-VT. In a scenario of normal water availability, this information is very useful for the authorization by the WUA for the second and third irrigation since these should coincide with stages V6-V8 and V11-VT respectively as recommended by INIFAP (2017) and Ojeda-Bustamante *et al.* (2006); under restricted water availability scenarios, this approach can have greater relevance since the IM operated by a WUA has the recurrent need to optimize the number of needed irrigations

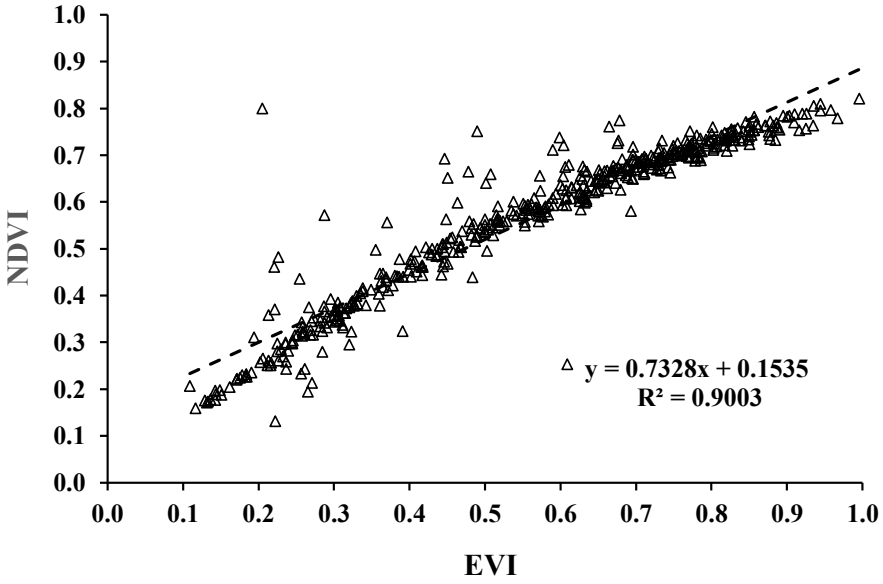

Figure 7. EVI-NDVI relationship using remote sensing corn data period 1998 to 2018 in the irrigation district (ID) 075.

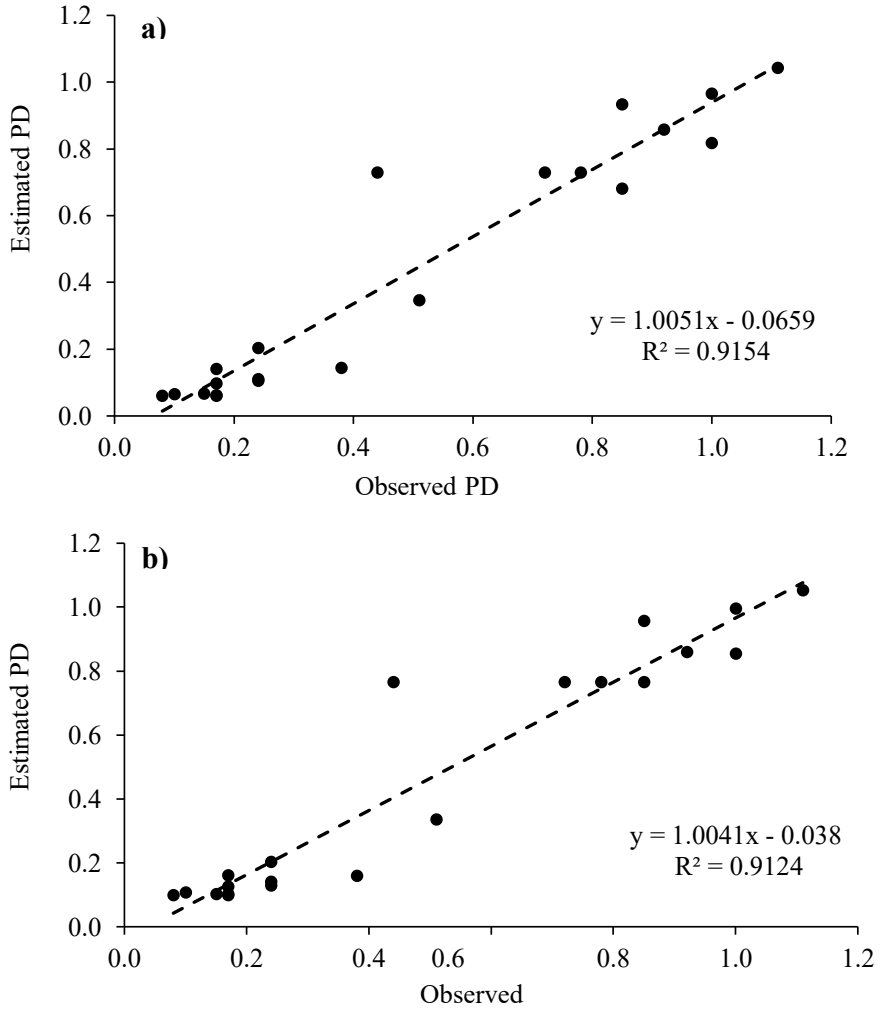

Figure 8. Relationship of observed and estimated phenological development (PD) in reference farms for the Autum-Winter (AW) 2017-2018 season. Spectral model NDVI (a) and EVI (b) in irrigation district (ID) 075, north of the state of Sinaloa, Mexico.

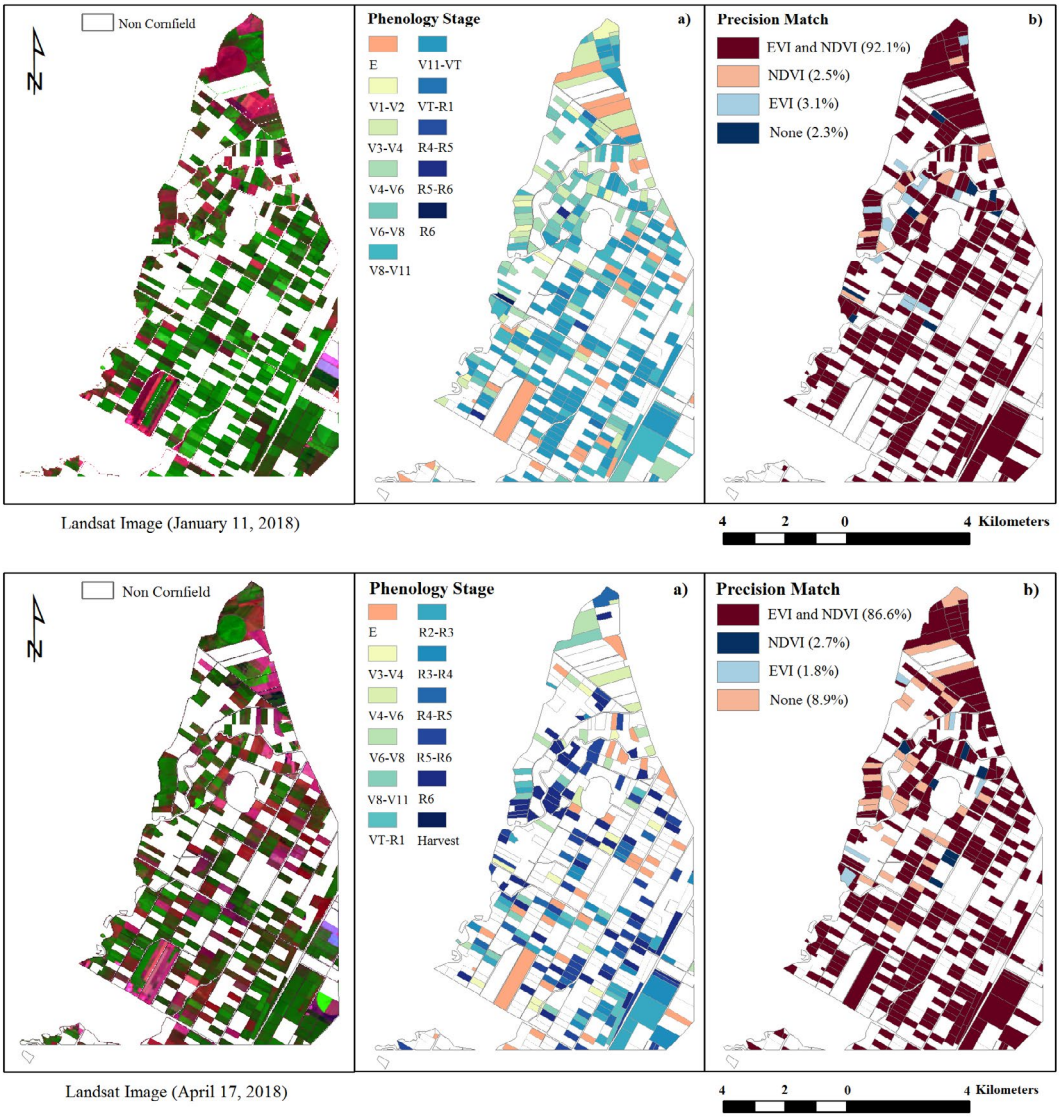

Figure 9. Observed corn phenology (a), spectral model's precision using NDVI and EVI (b) on January 11 2018 (above) and April 17 2018 (below), in irrigation module (IM) Batequis.

and distribute them in the most sensitive phases to water stress without affecting the yield. The validation in this date indicated that compared with the actual phenology, 92.1% of the farms coincided with that generated by both spectral models, 2.5% with NDVI model, 3.1% with EVI model and 2.3% with neither model.

On the second date (April 17, 2018) as Fig. 9 (below) shows, the predominant phases were from R2-R3 to R6 and farms close to being harvested. This is important to schedule the last irrigation and to estimate farms close to phenological maturity. The validation indicated that compared with the actual phenology, 86.6% of the monitored farms coincided with the phenology generated from both models, 2.7% with the NDVI model, 1.8% with EVI model and 8.9% with neither model. This decrease in precision of the models and the increase of the error with respect to the first date may be due to the presence of harvested farms o in senescence, with weeds and the effect of clouds, as reported by Whitcraft *et al.* (2015).

Conclusions

The spatio-temporal inter and intra-seasonal variability of corn phenological development, justifies the use of remote sensing data to monitor crops over large agricultural areas. The historical behavior of two VIs (NDVI and EVI), associated with the phenological development (PD), showed differences in the early and late stages of development, having EVI higher sensitivity. An algorithm and methodology for monitoring corn phenology on large scale using both field data and remote sensing data were generated and integrated with the GIS-based phenology monitoring. The validation of the methodology

in reference fields indicated an acceptable correlation between the observed PD and the estimated PD for the two VIs with R^2 = 0.9154 and 0.9124 for NDVI an EVI respectively, and RMSE values of 0.1307 for NDVI and 0.1219 for EVI, however, the effect of point´s dispersion and spatial variability was also observed, which can be reduced by using homogeneous areas. On the other hand, the validation of methodology at large-irrigated scale, using field data on two contrasting dates, was more practical and precise due to the points dispersion effect was reduced by using values interval. This model indicated that at the beginning of the crop season the precision to monitoring the phenological phases was of more than 92% with the two VIs and decreased to 86.6% in the end crop season, mainly due to the presence of harvested farms with bare soil o in senescence.

Acknowledgements

The authors thank the Instituto Mexicano de Tecnología del Agua (IMTA) for its support for doctoral studies, to the Fondo Sectorial SADER-CONACYT within the framework of the project “Plataforma WEB informativa sobre usos del agua en la agricultura nacional” for granting academic scholarships to undergraduate students to support this study, and the Instituto Nacional de Investigaciones Forestales Agrícolas y Pecuarias (INIFAP) for its support in the fieldwork.

References

Burke M, Lobell DB, 2017. Satellite-based assessment of yield variation and its determinants in smallholder African systems. Proc Natl Acad Sci 114 (9): 2189-2194. https://doi.org/10.1073/pnas.1616919114

Castillo CM, Ibáñez CLA, 2017. Análisis de sequías meteorológicas en la cuenca del río Fuerte, México. Tecnología y Ciencias del Agua VIII (1): 35-52. https://doi.org/10.24850/j-tyca-2017-01-03

CONAGUA, 2019a. Estadísticas agrícolas de los distritos de riego. https://www.gob.mx/conagua/documentos/estadisticas-agricolas-de-los-distritos-de-riego

CONAGUA 2019b. Estadísticas agrícolas de unidades de riego. https://www.gob.mx/conagua/documentos/estadisticas-agricolas-de-unidades-de-riego https://www.gob.mx/conagua/documentos/estadisticas-agricolas-de-unidades-de-riego

Chander G, Markham BL, Helder DL, 2009. Summary of current radiometric calibration coefficients for Landsat MSS, TM, ETM+, and EO-1 ALI sensors. Remote Sens Environ 113: 893-903. https://doi.org/10.1016/j.rse.2009.01.007

De Bernardis C, Vicente G-Guijalba F, Martinez-Marin T, López-Sanchez JM, 2016. Particle filter approach for real-time estimation of crop phenological states using time series of NDVI images. Remote Sens 8: 610. https://doi.org/10.3390/rs8070610

Espinosa EJL, Palacios VE, Tijerina ChL, Flores MH, Quevedo NA, 2017. Sistema de monitoreo satelital para el seguimiento y desarrollo de cultivos del Distrito de Riego 038. Tecnología y Ciencias del Agua VIII (1): 95-104. https://doi.org/10.24850/j-tyca-2017-01-07

Flores-Gallardo H, Ojeda-Bustamante W, Flores-Magdaleno H, Mejía-Sáenz E, Sifuentes-Ibarra E, 2012. Grados día y la programación integral del riego en el cultivo de papa. Terra Latinoamericana 30 (1): 59-67.

Ghamghami M, Nozar G, Irannejad P, Ghorbani K, 2019. Comparison of data mining and GDD-based models in discrimination of corn phenology. Int J Plant Prod 13 (1): 11-22. https://doi.org/10.1007/s42106-018-0030-2

Heupel K, Spengler D, Itzerott S, 2018. A progressive crop-type classification using multitemporal remote sensing data and phenological information. J Photogram Remote Sens Geoinform Sci 86: 53-69. https://doi.org/10.1007/s41064-018-0050-7

Huete AR, Didan K, Miura T, Rodríguez EP, Gao X, Ferreira G, 2002. Overview of the radiometric and biophysical performance of the MODIS vegetation indices. Remote Sens Environ 83: 195-213. https://doi.org/10.1016/S0034-4257(02)00096-2

Hufkens K, Melaas EK, Mann ML, Foster T, Ceballos F, Robles M, Kramer B, 2019. Monitoring crop phenology using a smartphone based near-surface remote sensing approach. Agr Forest Meteorol 265: 327-337. https://doi.org/10.1016/j.agrformet.2018.11.002

INIFAP, 2017. Agenda Técnica Agrícola Sinaloa. Instituto Nacional de Investigaciones Forestales, Agrícolas y Pecuarias. Ciudad de México, México. 209 pp.

Jensen JR, 2007. Remote sensing of the environment: an earth resource perspective, 2nd ed Prentice Hall series in geographic information science, USA. ISBN 0-13-188950-8. 592 pp.

Kamble B, Kilic A, Hubbard K, 2013. Estimating crop coefficients using remote sensing-based vegetation index. Remote Sens 5: 1588-1602. https://doi.org/10.3390/rs5041588

Kimball BA, White JW, Wall GW, Ottman MJ, 2012. Infrared-warmed and unwarmed wheat vegetation indices coalesce using canopy-temperature-based growing degree days. Agron J 104 (1): 114-118. https://doi.org/10.2134/agronj2011.0144

Liao CH, Wang J, Dong T, Shang J, Liu J, Song Y, 2019. Using spatio-temporal fusion of Landsat-8 and MODIS data to derive phenology, biomass and yield estimates

for corn and soybean. Sci Total Environ 650: 1707-1721. https://doi.org/10.1016/j.scitotenv.2018.09.308

Matsushita B, Yang W, Chen J, Onda Y, Qiu G, 2007. Sensitivity of the enhanced vegetation index (EVI) and normalized difference vegetation index (NDVI) to topographic effects: A case study in high-density cypress forest. Sensors 7: 2636-2651. https://doi.org/10.3390/s7112636

Mavi HS, Tupper GJ, 2004. Temperature and crop production. In: Agrometeorology: principles and applications of climate studies in agriculture, Chapter 3, pp: 43-70. The Haworth Press Inc., NY. https://doi.org/10.1201/9781482277999

NASA, 2019. Landsat image gallery. https://landsat.visibleearth.nasa.gov/

Ojeda-Bustamante W, Sifuentes-Ibarra E, Unland-Weiss H, 2006. Programación integral del riego en maíz en el norte de Sinaloa, México. Agrociencia (Mexico) 40 (1): 13-25.

Ojeda-Bustamante W, González-Camacho JM, Sifuentes-Ibarra E, Isidro E, Rendón-Pimentel L, 2007. Using spatial information systems to improve water management in Mexico. Agr Water Manage 89: 81-88. https://doi.org/10.1016/j.agwat.2006.11.002

Ojeda-Bustamante W, Sifuentes-Ibarra E, Ontiveros-Capurata RE, Iñiguez CM, Rojano AA, 2014. Proyecciones de cambio climático para el estado de Sinaloa. In: Sinaloa y el cambio climático global; Flores-Campaña LM *et al.* (eds), pp: 115-131. Instituto de Apoyo a la Investigación e Innovación y Universidad Autónoma de Sinaloa, Culiacán, Mexico.

QGIS, 2019. User Guide. Release 3.4. QGIS Project. https://www.qgis.org/en/docs.

Reed BC, Brown JF, Vanderzee DL, Thomas RM, James W, Ohlen DO, 1994. Measuring phenological variability from satellite imagery. J Veg Sci 5: 703-714. https://doi.org/10.2307/3235884

Ritchie SW, Hanway JJ, Benson GO, 1992. How a corn plant develops. Special report 48 (rev.). Iowa State University. Coop. Ext. Serv., Ames, IA, USA.

Roth GW, Yocum JO, 1997. Use of hybrid growing degree day ratings for corn in the northeastern USA. J Prod Agr 10: 283-288. https://doi.org/10.2134/jpa1997.0283

Rouse JW, Haas RH, Schell JA, Deering DW, 1974. Monitoring vegetation systems in the great plains with ERTS. Proc Third Earth Resources Technology Satellite-1 Symp. Greenbelt: NASA SP-351, 3010-3017.

SIAP, 2019. Avance de siembras y cosechas. Servicio de Información Agroalimentaria y Pesquera, Gobierno de Mexico.

Sifuentes E, Macías J, Ruelas JR, Preciado P, Ojeda W, Inzunza MA, Samaniego JA, 2015. Mejoramiento del grado de uso del nitrógeno en maíz, mediante técnicas parcelarias de riego por superficie. Rev Mex Cienc Agr 6 (8): 1903-1914. https://doi.org/10.29312/remexca.v6i8.528

Teal RK, Tubana BS, Girma K, Freeman KW, Arnall DB, Walsh O, 2006. In-season prediction of corn grain yield potential using normalized difference vegetation index. Agron J 98: 1488-1494. https://doi.org/10.2134/agronj2006.0103

Tsouros DC, Bibi S, Sarigiannidis PG, 2019. A review on UAV-based applications for precision agriculture. Information 10 (11): 349. https://doi.org/10.3390/info10110349

UAS, 2014. Sinaloa ante el cambio climático global; Flores Campiña LM *et al.*, Ed. Universidad Autónoma de Sinaloa, México. ISBN: 978-607-737-051-2. 385 pp.

USGS, 2018. USGS Global visualization viewer (Glovis). United States Geological Survey. https://glovis.usgs.gov/

USGS, 2019. Landsat 8 (L8) data users handbook Version 4.0. United States Geological Survey, Sioux Falls, SD, USA.

Viña A, Gitelson AA, Rundquist DC, Keydan G, Leavitt B, Schepers J, 2004. Monitoring corn (*Zea mays* L.) phenology with remote sensing. Agron J 96: 1139-1147. https://doi.org/10.2134/agronj2004.1139

Wei Y, Tong X, Cheng G, Liu D, Han Z, 2019. Remote detection of large-area crop types: The role of plant phenology and topography. Agriculture 9 (7): 150. https://doi.org/10.3390/agriculture9070150

Whitcraft AK, Vermote EF, Becker RI, Justice CO, 2015. Cloud cover throughout the agricultural growing season: impacts on passive optical earth observations. Remote Sens Environ 156: 438-447. https://doi.org/10.1016/j.rse.2014.10.009

Zhong L, Gong P, Biging GS, 2014. Efficient corn and soybean mapping with temporal extendability: a multi-year experiment using Landsat imagery. Remote Sens Environ 140: 1-13. https://doi.org/10.1016/j.rse.2013.08.023